INORGANIC CHEMISTRY
FRONTIERS

RESEARCH ARTICLE

View Article Online
View Journal | View Issue

Cite this: *Inorg. Chem. Front.*, 2022, **9**, 1714

Pyrazine functionalization to boost the antenna effect in rare-earth metal–organic frameworks for tetracycline detection†

Kun Wu, ‡[a] Xin-Yi Liu,‡[a] Yong-Liang Huang, [b] Mo Xie, [a] Xiao Xiong, [a] Ji Zheng, [a] Weigang Lu *[a] and Dan Li *[a]

Here we report a generalizable strategy for the synthesis of rare-earth metal–organic frameworks (RE-MOFs) with 12-connected RE_9 clusters and **shp** topology. A total of 26 isostructural RE-MOFs (**JNU-205-RE** and **JNU-206-RE**) were obtained from two X-shaped tetracarboxylate linkers, 4,4′,4″,4‴-benzene-2,3,5,6-tetrayl-tetrabenzoate (BTEB) and 4,4′,4″,4‴-pyrazine-2,3,5,6-tetrayl-tetrabenzoate (BTTB). Among them, the two europium-based RE-MOFs (**JNU-205-Eu** and **JNU-206-Eu**) were observed to show characteristic red luminescence of Eu^{3+}, indicating the antenna effect of both linkers for Eu^{3+} sensitization. Interestingly, the one constructed with a pyrazine-centered BTTB linker (**JNU-206-Eu**) exhibited a luminescence quantum yield 120 times that of the one constructed with a benzene-centered BTEB linker (**JNU-205-Eu**). We suspect pyrazine functionalization renders the antenna linker not only more electron rich but also with better conjugation, facilitating energy transfer from the linker to the metal and therefore leading to efficient Eu^{3+} sensitization. As a result, the luminescence quenching sensitivity of **JNU-206-Eu** for tetracyclines (TCs) was improved by a factor of 3 with a detection limit comparable to those of the best-performing MOF materials reported so far. Experimental data and theoretical calculations suggest the quenching mechanism be mainly ascribed to the internal filtration effect (IFE). Furthermore, a mixed matrix film by dispersion of **JNU-206-Eu** crystalline powders on a polycaprolactone sheet was applied to demonstrate rapid and visualizable luminescence response towards TCs with good reusability in aqueous solutions.

Received 27th January 2022,
Accepted 17th February 2022

DOI: 10.1039/d2qi00214k

rsc.li/frontiers-inorganic

1. Introduction

Antibiotics have a history of being used to fight bacterial infections for nearly a hundred years.[1,2] Yet their uncontrolled use has led to the spread of antibiotic-resistant bacteria, which is widely considered to be the next global pandemic.[3] For example, tetracyclines (TCs), owing to their broad-spectrum antibacterial activity and low toxicity, have been extensively used in animal production and breeding to promote growth and improve immunity.[4–6] The overly used TCs may be introduced into domestic water during the discharge process, increasing the presence of drug-resistant bacteria in the environment. Meanwhile, trace amounts of TCs that remain in livestock and poultry may cause human pathogens to develop antibiotic resistance.[7] Hence, it is of paramount importance to not only strengthen the regulation of the proper use of antibiotics but also to keep track of antibiotic residues in food and the environment to ensure compliance with safety standards. Currently, the testing of antibiotics is mainly done through high-performance liquid chromatography (HPLC), microbiological assay (MBA), gas-phase/liquid phase-mass spectrometry (GC/LC-MS) and immunoassay (IA), which are rather expensive and time-consuming.[8–12] Thus, developing affordable testing tools for on-site real-time antibiotic detection is necessary and urgent.

Metal–organic frameworks (MOFs) are crystalline porous coordination polymers assembled with metal ions and organic linkers. Due to their abundant pore metrics and surface chemistry, MOFs have been widely studied in host–guest recognition, LED lighting, catalysis, information storage and gas storage/separation, *etc.*[13–27] As far as luminescence sensing is concerned, rare-earth MOFs (RE-MOFs) are promising candidates owing to their intriguing electronic/optical properties,

[a]*College of Chemistry and Materials Science, and Guangdong Provincial Key Laboratory of Functional Supramolecular Coordination Materials and Applications, Jinan University, Guangzhou 510632, P. R. China. E-mail: weiganglu@jnu.edu.cn, danli@jnu.edu.cn*
[b]*Department of Chemistry, Shantou University Medical College, Shantou, Guangdong 515041, P. R. China*

†Electronic supplementary information (ESI) available: Experimental details, physical measurements, and crystal structure data. See DOI: 10.1039/d2qi00214k

‡These authors contributed equally to this work.

intense luminescence emissions and high resistance to interference.[28–32] However, the production of RE-MOFs with characteristic RE luminescence is still serendipitous, and the limited hydrolytic stability of most RE-MOFs hinders their real-world applications in aqueous-medium environments. Therefore, it is equally important to prepare RE-MOFs of high stability and intense emission if they are to be used for on-site luminescence sensing. Note that the 4f–4f electron transition of RE metal is forbidden according to the Laporte rule,[33] and direct excitation of RE metal only yields weak emission. To solve this issue, chromophores with strong absorption capacity are often integrated into the RE-MOFs as linkers for sensitizing the RE ions through energy transfer. This process of RE sensitization for their characteristic emission is known as the "antenna effect".[34–36]

Herein, we report a generalizable strategy for the synthesis of highly stable RE-MOFs with **shp** topology and 12-connected RE_9 clusters. By adjusting the dosage of the modulating reagent (2-fluorobenzoic acid), a total of 26 isostructural RE-MOFs, **JNU-205-RE** and **JNU-206-RE** (JNU = Jinan University; RE = Eu, Pr, Nd, Sm, Gd, Tb, Dy, Ho, Er, Tm, Yb, Lu and Y), were obtained with X-shaped tetracarboxylate linkers, 4,4′,4″,4‴-benzene-2,3,5,6-tetrayl-tetrabenzoate (BTEB) and 4,4′,4″,4‴-pyrazine-2,3,5,6-tetrayl-tetrabenzoate (BTTB). The excellent hydrolytic stability of these RE-MOFs could be attributed to the high connectivity of RE_9 clusters, which may shield from attack by water. Luminescence studies revealed characteristic red emission of Eu^{3+} for **JNU-205-Eu** and **JNU-206-Eu**, indicating the antenna effect of both linkers and Eu^{3+} sensitization. Interestingly, an over 120-fold increase in luminescence quantum yield was observed for **JNU-206-Eu** in comparison with **JNU-205-Eu**. We suspect pyrazine functionalization renders the antenna linker more electron rich and with better conjugation, therefore leading to a boosted antenna effect and efficient energy transfer from linker to Eu^{3+}. As a result, the luminescence quenching sensitivity of **JNU-206-Eu** for tetracyclines (TCs) is three times higher than that of **JNU-205-Eu**. In addition, experimental characterizations and theoretical calculations were performed and the luminescence quenching was mainly attributed to the internal filtration effect (IFE).

2. Results and discussion

2.1. Synthesis of JNU-205-RE/JNU-206-RE

Solvothermal reactions of $RE(NO_3)_3{\cdot}6H_2O$, H_4BTEB/H_4BTTB and the modulating reagent (2-fluorobenzoic acid) in *N*,*N*-dimethylformamide (DMF) afforded colorless hexagonal-prismatic crystals of **JNU-205-RE**/**JNU-206-RE**. Taking **JNU-206-RE** as an example, 13 isostructural RE-MOFs amenable to single crystal X-ray diffraction (SCXRD) analysis were obtained by adjusting the dosage of 2-fluorobenzoid acid (please refer to ESI† for details), except for Sc, La and Ce (Pm salt is not commercially available). Our experimental results showed that, instead of M_9 clusters, Sc, La and Ce have a tendency to form a one-dimensional rod, a single-atom node and M_6 clusters, respectively, which is consistent with the literature.[37–41]

2.2. Structure characterization

Taking **JNU-206-RE** as an example, SCXRD studies disclose that **JNU-206-RE** crystallized in a primitive hexagonal space group with $P6_3/mmc$ or $P\bar{3}m1$ symmetry. Analysis of the crystal structure unveils a three-dimensional (3D) framework with **shp** topology built from $[RE_9(\mu_3\text{-}O)_2(\mu_3\text{-}OH)_{12}(OH)_2(H_2O)_{12}(COO)_{12}]$ SBUs and tetracarboxylate linkers. As shown in Fig. 1, each BTTB linker is connected by four RE_9 clusters through its benzoate arms, while each RE_9 cluster is connected by twelve BTTB linkers. Further analysis of the RE_9 cluster reveals that there are two crystallographically independent RE atoms (RE1 and RE2) in **JNU-206-RE** (Fig. S3 and S4†). RE1 is coordinated with four O atoms from four carboxylates of four BTTB linkers,

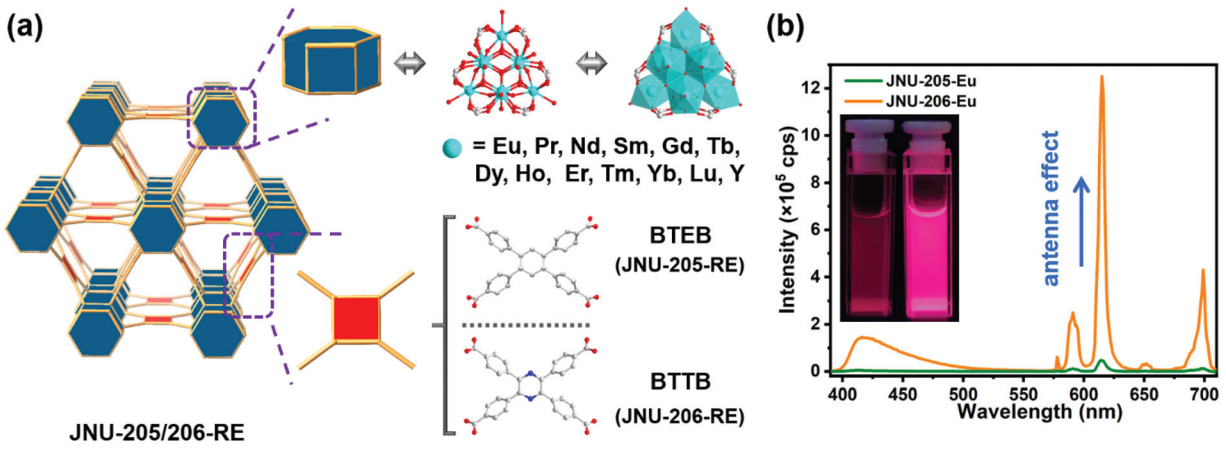

Fig. 1 (a) Crystal structure of **JNU-205-RE**/**JNU-206-RE** and tiling representation of the **shp** topology built from a 12-connected RE_9-cluster and a 4-connected BTEB/BTTB linker (sky blue for RE, red for O, gray for C and blue for N; H atoms are omitted for clarity). (b) Comparison of emission spectra of aqueous suspensions of **JNU-205-Eu** and **JNU-206-Eu** (30 mg per 100 mL, λ_{ex} = 365 nm, slit = 1 nm). Inset: photographs of aqueous suspensions of **JNU-205-Eu** (left) and **JNU-206-Eu** (right) under 365 nm UV lamp.

four μ_3-O/μ_3-OH and one H_2O. RE2 is coordinated with two O atoms from two carboxylates of two BTTB linkers, five μ_3-O/μ_3-OH and one H_2O. Overall, three RE1 and six RE2 are assembled with fourteen μ_3-O/μ_3-OH, nine H_2O and twelve carboxylates to form a hexagonal prismatic RE_9 cluster.

2.3. Porosity and stability

Taking **JNU-205-Eu** and **JNU-206-Eu** as examples, the as-synthesized crystals were immersed in water for three days, solvent exchanged with DMF and EtOH in turn for another two days and then heated to 120 °C overnight before N_2 adsorption/desorption measurements. As shown in Fig. 2a, Type I adsorption isotherms were observed for **JNU-205-Eu** and **JNU-206-Eu**, suggesting that both have permanent microporosity. The Brunauer–Emmett–Teller (BET) surface area was calculated to be 1076 $m^2\ g^{-1}$ for **JNU-205-Eu** and 1125 $m^2\ g^{-1}$ for **JNU-206-Eu** based on their respective data points on the adsorption isotherm branches. The percentages of guest accessible volume for **JNU-205-Eu** and **JNU-206-Eu** are 49.8 and 49.6%, respectively, as calculated using PLATON. The chemical stability of **JNU-205-Eu** and **JNU-206-Eu** was validated using the retained PXRD patterns after their bulk samples were immersed in aqueous solutions of different values of pH or in organic solvents for 24 h (Fig. 2b, S59, and S60†). In addition, the thermal stability was investigated using thermogravimetric analysis (TGA) over a temperature range of 40–800 °C under an N_2 atmosphere (Fig. S58†), and variable temperature powder X-ray diffraction (VT-PXRD) data further confirm their thermal stability (Fig. S61†) on account of the retained peak locations and intensities.

2.4. Luminescence studies

2.4.1. Antenna effect in JNU-205-Eu and JNU-206-Eu. Among the 26 RE-MOFs synthesized in this work, the two europium-based RE-MOFs (**JNU-205-Eu** and **JNU-206-Eu**) exhibit the characteristic red luminescence of Eu^{3+}, indicating the antenna effect of both linkers for Eu^{3+} sensitization. For example, the emission spectrum of **JNU-205-Eu** shows a set of typical Eu^{3+} emission peaks at 578, 591, 615, 649 and 695 nm ($^5D_0 \rightarrow {}^7F_J$, J = 0–4, Fig. S75 and S76†) as well as the emission peak of the BTEB linker at 428 nm (Fig. S77 and S78†).[42,43] However, the luminescence quantum yield (QY) and emission intensity of **JNU-205-Eu** are lower than those of many of the reported Eu-MOFs, likely due to the less efficient absorption of excitation light from the BTEB linker. To boost the antenna effect, we decided to use pyrazine functionalization to promote energy transfer from the linker to the metal. As expected, the emission intensity of **JNU-206-Eu** was significantly increased. It exhibits bright red luminescence under irradiation at 254 and 365 nm with CIE coordinates of (0.49, 0.26) and (0.40, 0.18), respectively (Fig. S79†). The QYs of **JNU-205-Eu** and **JNU-206-Eu** were calculated to be 0.2 and 25.6%, respectively, an over 120-fold increase after pyrazine functionalization. As depicted in Fig. S81,† the dihedral angle between the benzoate ring and the central pyrazinyl ring in **JNU-206-Eu** is 56.8°, whereas the dihedral angle between the benzoate ring and the central phenyl ring in **JNU-205-Eu** is 60.2°. Therefore, the increase in QY and emission intensity of **JNU-206-Eu** can be partially attributed to the better conjugation of the linker upon pyrazine functionalization. Furthermore, H_4BTTB is known to be an aggregation-induced emission (AIE) molecule.[30,44] Organic molecules with AIE effect usually exhibit stronger luminescence intensity after being integrated into the framework owing to the restricted intramolecular rotation (RIR).[30,44–46] For instance, the luminescence intensity of **JNU-206-Gd** (the one constructed with the BTTB linker but no antenna effect) was indeed considerably increased in comparison with H_4BTTB (Fig. S80†).

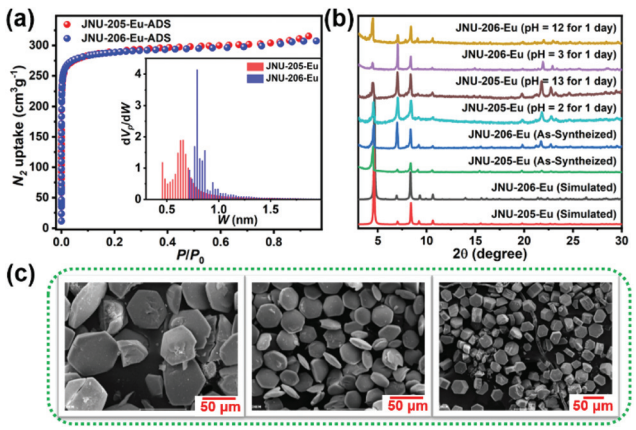

Fig. 2 (a) N_2 adsorption isotherms of **JNU-205-Eu** and **JNU-206-Eu** at 77 K. Inset shows pore size distribution plots according to the HK method. (b) Comparison of the simulated PXRD patterns with the experimental ones of the as-synthesized **JNU-205-Eu**/**JNU-206-Eu** and after being treated with base (pH = 12, 13) or acid (pH = 2, 3) for one day. (c) Representative desktop scanning electron microscope (SEM) images of **JNU-206-Eu** (left), **JNU-206-Y** (middle) and **JNU-206-Nd** (right).

2.4.2. Luminescence sensing of TCs in water. The excellent hydrolytic stability and luminescence properties of **JNU-206-Eu** prompted us to explore its application for sensing TCs, including oxytetracycline (OTC), tetracycline (TC) and chlortetracycline (CTC) in aqueous solutions. Luminescence titrations were performed and all the emission peaks of **JNU-206-Eu** were observed to gradually decrease upon the addition of OTC, TC or CTC (Fig. S82†), indicating the luminescence quenching of **JNU-206-Eu** for TCs. Taking OTC as an example, the luminescence emission spectra and, particularly, the peak intensities at 615 nm were collected as an OTC solution was titrated into an aqueous suspension of **JNU-206-Eu**. The luminescence quenching efficiency can be quantitatively described by the Stern–Volmer (S–V) equation: $I_0/I = 1 + K_{sv}[M]$, where K_{sv} is the quenching constant (M^{-1}), [M] is the molar concentration of OTC and I_0 and I are the luminescence intensities (at 615 nm) before and after the addition of OTC, respectively. As shown in Fig. 3a–c, the S–V plots for TCs are in good linear relationships at low concentrations. The K_{sv} values were calculated to be $2.37 \times 10^4\ M^{-1}$ (R^2 = 0.987) for OTC, $2.37 \times 10^4\ M^{-1}$ (R^2 = 0.996) for TC and $1.33 \times 10^4\ M^{-1}$ (R^2 = 0.990) for CTC from their respective concentration-dependent emission spectra. The

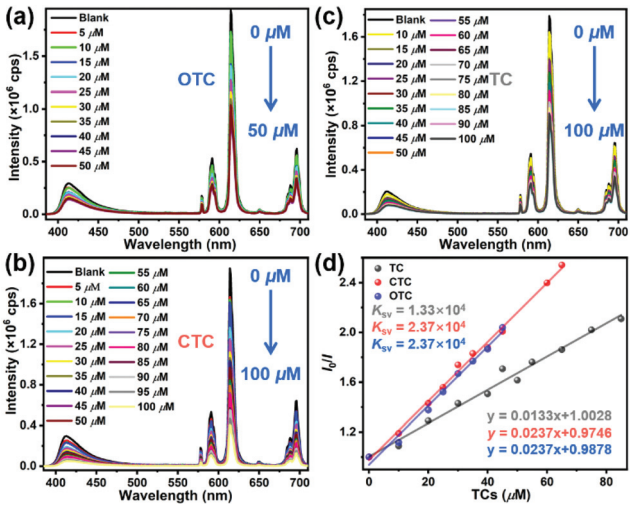

Fig. 3 (a–c) Concentration-dependent luminescence emission spectra of aqueous suspensions of **JNU-206-Eu** upon incremental addition of OTC, CTC and TC. (d) S–V plots of I_0/I *versus* concentrations of OTC, CTC and TC (λ_{ex} = 365 nm).

limits of detection (LODs) of **JNU-206-Eu** for OTC, CTC and TC were calculated to be 0.35, 0.36 and 0.62 μM, respectively (LOD = $3S_b/K_{sv}$, where S_b is the standard deviation of the blank solutions). These values are higher than most of those reported in porous materials (Table S15†).

As a comparison, **JNU-205-Eu** was also used as a luminescence probe for OTC sensing. Not surprisingly, the LOD of **JNU-205-Eu** for OTC was calculated to be 1.07 μM (Fig. S84†), much less sensitive than that of **JNU-206-Eu**. The lower LOD of **JNU-206-Eu** for OTC can be mainly attributed to its significantly increased emission intensity due to the boosted antenna effect of pyrazine functionalization (Fig. 1). In addition, we suspect the pyrazine functionalization may increase the host–guest interaction and provide strong adsorption sites for OTC accumulation, thus further lowering its detection limit.

2.4.3. Recycling performance of JNU-206-Eu. Reusability is an important parameter that should be evaluated for luminescence probes. As mentioned above, **JNU-206-Eu** exhibited excellent acid/base, solvent and thermal stability, which is a prerequisite for its use in multicycle detection. Moreover, the luminescence of **JNU-206-Eu** can be easily recovered by soaking in 95% ethanol, and the regenerated **JNU-206-Eu** can be reused for the luminescence sensing of OTC without compromising sensitivity. After five cycles of sensing experiments, the quenching efficiency was almost the same (Fig. S86†), indicating the practicability of **JNU-206-Eu** for OTC sensing. Moreover, the peak locations on the PXRD patterns of **JNU-206-Eu** remained the same after being immersed in a highly concentrated OTC solution for three days, further emphasizing its potential as a viable candidate for OTC sensing in aqueous solutions (Fig. S87†).

2.4.4. Selective detection of OTC, TC and CTC. To assess the selectivity of **JNU-206-Eu** for TCs in the presence of other antibiotic species, we carried out luminescence experiments with several other antibiotics, such as erythromycin (ERY), vancomycin (VA), griseofulvin (GRI), chloramphenicol (CHL), sulfamethazine (SMM) and sulfathiazole (STZ), as interference. **JNU-206-Eu** was ground and ultrasonically dispersed in deionized water (30 mg per 100 mL) before use. Luminescence emission was monitored when 0.3 mL of antibiotic solution (0.5 mM) was added to 2.7 mL of the suspension solution of **JNU-206-Eu**. As shown in Fig. 4 and S87–S89,† the emission intensity of **JNU-206-Eu** at 615 nm did not show any obvious decrease upon addition of the selected interfering antibiotics, while it was significantly reduced when OTC, TC or CTC was added. The results further demonstrate the potential of **JNU-206-Eu** for the selective detection of TCs in the presence of other antibiotic species. Subsequently, we also carried out multicycle sensing experiments in the presence of interfering antibiotics, and the quenching efficiency of **JNU-206-Eu** was not disturbed after five cycles (Fig. S90†).

2.4.5. Luminescence quenching mechanism. Studies have shown that prevailing luminescence sensing mechanisms for MOF-based materials include fluorescence resonance energy transfer (FRET), photoinduced electron transfer (PET), structural conversion (SC), the internal filtration effect (IFE), chemical conversion (CC) and dynamic/static quenching (D/SQ).[12,28,29,31] To better understand the luminescence quenching mechanism of **JNU-206-Eu** for TCs, combined experimental characterizations and theoretical calculations were carried out. Taking OTC as an example, PXRD patterns of **JNU-206-Eu** were measured to confirm the retention of its phase purity after being soaked in an aqueous solution of OTC for three days (Fig. S86†), excluding luminescence quenching from the decomposition and/or collapse of the **JNU-206-Eu** framework.[13,47] The UV–visible absorption spectrum of OTC and the excitation spectrum of **JNU-206-Eu** were broadly superimposed in the range of 270–400 nm (Fig. 5a), indicative of strong competitive absorption for excitation light between **JNU-206-Eu** and OTC. Therefore, the luminescence quenching of **JNU-206-Eu** for OTC could be mainly attributed to IFE.[48] Nevertheless, energy transfer from **JNU-206-Eu** to OTC cannot

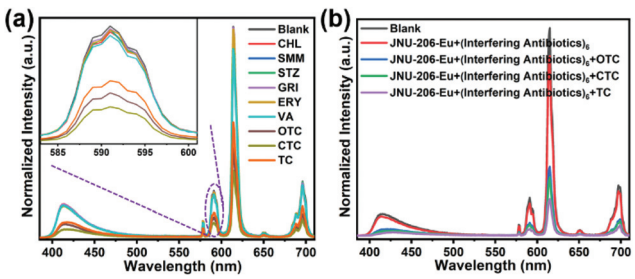

Fig. 4 (a) Luminescence emission spectra of aqueous suspensions of **JNU-206-Eu** (30 mg per 100 mL) in the presence of different antibiotics (0.5 mM) (λ_{ex} = 365 nm). (b) Luminescence emission spectra of aqueous suspensions of **JNU-206-Eu** (30 mg per 100 mL) in the presence of six interfering antibiotics (each 0.5 mM) and further addition of OTC, CTC or TC (0.5 mM), respectively (λ_{ex} = 365 nm).

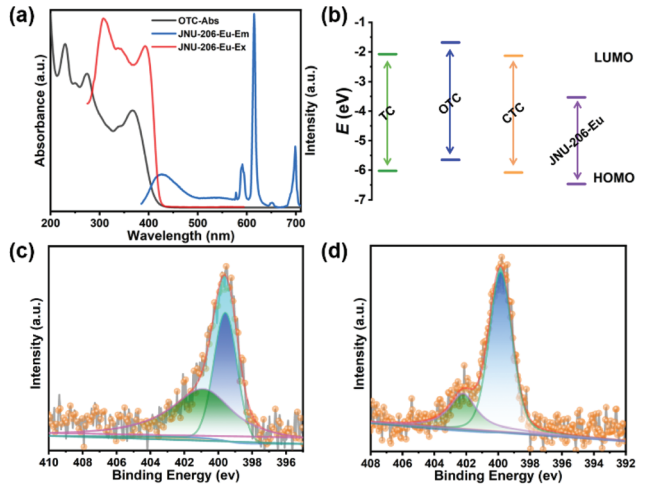

Fig. 5 (a) UV–visible absorption spectrum of OTC, excitation and emission spectra of **JNU-206-Eu**. (b) Schematic depiction of the frontier orbital energy levels of OTC, TC, CTC and **JNU-206-Eu**. (c), (d) N 1s XPS spectra of **JNU-206-Eu** and **JNU-206-Eu-OTC**.

be completely excluded, as a slight overlap was observed between the UV–visible absorption spectrum of OTC and the luminescence emission spectrum of **JNU-206-Eu** (Fig. 5a).

To investigate the possibility of a PET process, the highest occupied molecular orbital (HOMO) and the lowest unoccupied molecular orbital (LUMO) energy levels of OTC, TC and CTC were calculated using density functional theory (DFT) at the B3LYP/def2-tzvp level.[49] On the other hand, a cyclic voltammetry (CV) experiment was performed to assess the LUMO level of **JNU-206-Eu**, and the UV–visible diffuse reflectance spectrum (UV–DRS) was collected to calculate its optical band gap. The HOMO level was thus estimated to be −6.47 eV on account of the band gap energy equation ($E_g = E_{HOMO} - E_{LUMO}$, Fig. S92–94†). As shown in Fig. 5b, all the LUMO energy levels of TC, OTC and CTC are higher than that of **JNU-206-Eu**, suggesting that luminescence responses are unlikely to be initiated by a PET process. Also, after the addition of OTC, the luminescence lifetime of **JNU-206-Eu** showed no obvious changes (0.315 *vs.* 0.318 ns; Fig. S95 and S96†), indicating a static quenching mechanism of **JNU-206-Eu** for its luminescence sensing of OTC.[50]

Additionally, high-resolution X-ray photoelectron spectroscopy (XPS) spectra of **JNU-206-Eu-TCs** (**JNU-206-Eu** after being soaked in OTC, TC and CTC solutions) showed that the Eu 3d peaks were shifted in comparison with those of **JNU-206-Eu** (Fig. S97†), suggesting weak interactions between Eu_9 clusters and TCs. Furthermore, the intensities of N 1s peaks at 402 eV were significantly enhanced for **JNU-206-Eu-TCs**, indicating relatively strong interactions (N···H–C, N···H–N, and N···H–O) between BTTB linkers and TCs (Fig. 5c, d, and S99†). These results corroborate our speculation that pyrazine-functionalized linkers in **JNU-206-Eu** provide strong adsorption sites for the accumulation of TCs, which may increase the luminescence quenching sensitivity.

2.5. Mixed matrix films for visualizable sensing

To investigate the practical application of **JNU-206-Eu**, mixed matrix films were prepared and used for the visualizable sensing of TCs. **JNU-206-Eu** was dispersed in the biocompatible and biodegradable polymer (polycaprolactone, PCL) matrix to form a **JNU-206-Eu**-loaded PCL film.[51] The obtained **JNU-206-Eu-PCL** film was cut into strips and its sensing capacity for TCs tested (Fig. 6a). As demonstrated in Fig. 6b, the red emission of the strip was completely quenched upon contact with an aqueous solution of OTC under 365 nm UV light irradiation. To further evaluate the recycling performance of **JNU-206-Eu-PCL**, the **JNU-206-Eu-PCL** strip used was soaked in 95% ethanol for 1 min and then air-dried. The regenerated strip was again dipped into the OTC solution, while its luminescence emission was monitored. Remarkably, the emission intensity (615 nm) of **JNU-206-Eu-PCL** was retained after twenty cycles of sensing experiments (Fig. 6c), indicating the good practicability of **JNU-206-Eu-PCL** for sensing OTC in aqueous solutions. Furthermore, the capacity of **JNU-206-Eu-PCL** for sensing TC and CTC in aqueous solutions with good reusability was also demonstrated (Fig. S100 and 101†).

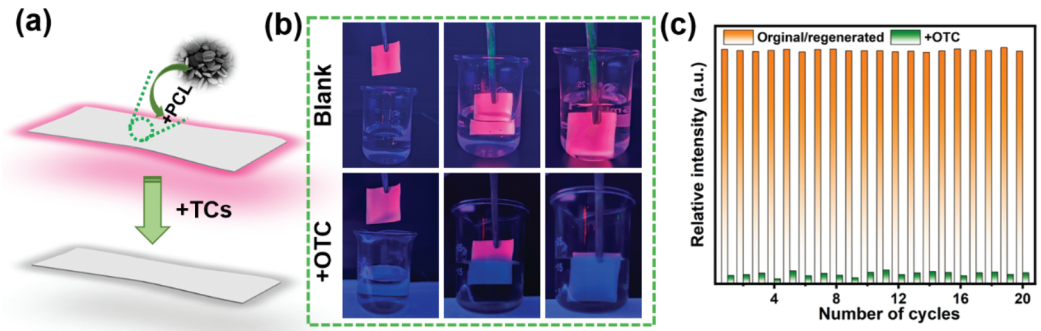

Fig. 6 (a) Illustration of the fabrication of a **JNU-206-Eu-PCL** strip and its application in sensing TCs; (b) photographs of **JNU-206-Eu-PCL** strips dipping into pure water (top) and aqueous solution of OTC (bottom); (c) 20 cycles of sensing experiments for OTCs and corresponding emission intensity (615 nm) of **JNU-206-Eu-PCL** (λ_{ex} = 365 nm).

3. Conclusion

We described herein a generalizable strategy for the synthesis of hydrolytically stable RE-MOFs with **shp** topology and a 12-connected RE_9-cluster. A total of 26 isostructural RE-MOFs (**JNU-205-RE** and **JNU-206-RE**) were obtained from two X-shaped tetracarboxylate linkers (BTEB and BTTB) by adjusting the dosage of the modulator (2-fluorobenzoic acid). Among them, **JNU-205-Eu** and **JNU-206-Eu** exhibit the antenna effect and red emission of Eu^{3+}. Interestingly, the red emission of **JNU-206-Eu** was much stronger, with a 120-fold increase in luminescence quantum yield compared with **JNU-205-Eu**, indicating that pyrazine functionalization in the BTTB linker significantly enhances the antenna effect and facilitates energy transfer from the linker to the metal. Luminescence titration experiments confirmed that the detection limit of our Eu-MOFs for TCs sensing was lowered by a factor of 3 upon pyrazine functionalization. In addition, a **JNU-206-Eu-PCL** strip was fabricated and demonstrated on-site real-time sensing of TCs in aqueous solutions. Overall, we have successfully illustrated a linker engineering strategy for boosting the antenna effect in Eu-MOFs and lowering the detection limit for luminescence sensing.

Conflicts of interest

There are no conflicts to declare.

Acknowledgements

This work was financially supported by the National Natural Science Foundation of China (nos 21731002, 21975104, 22101099 and 22150004), the Major Program of Guangdong Basic and Applied Research (2019B030302009), the Guangdong Basic and Applied Basic Research Foundation (no. 2020A1515011005), and the Special Fund Project for Science and Technology of Guangdong (STKJ2021172). We thank the high performance public computing service platform of Jinan University for providing computing resources.

Notes and references

1 R. Li, W. Wang, E.-S. M. El-Sayed, K. Su, P. He and D. Yuan, Ratiometric fluorescence detection of tetracycline antibiotic based on a polynuclear lanthanide metal–organic framework, *Sens. Actuators, B*, 2021, **330**, 129314.

2 M. Kumar, S. Jaiswal, K. K. Sodhi, P. Shree, D. K. Singh, P. K. Agrawal and P. Shukla, Antibiotics bioremediation: Perspectives on its ecotoxicity and resistance, *Environ. Int.*, 2019, **124**, 448–461.

3 L. Catteau, L. Zhu, F. Van Bambeke and J. Quetin-Leclercq, Natural and hemi-synthetic pentacyclic triterpenes as antimicrobials and resistance modifying agents against *Staphylococcus aureus*: A review, *Phytochem. Rev.*, 2018, **17**, 1129–1163.

4 J. Tarradas, N. Tous, E. Esteve-Garcia and A. J. Brufau, The control of intestinal inflammation: A major objective in the research of probiotic strains as alternatives to antibiotic growth promoters in poultry, *Microorganisms*, 2020, **8**, 148.

5 T. Morais, A. Inácio, T. Coutinho, M. Ministro, J. Cotas, L. Pereira and K. Bahcevandziev, Seaweed potential in the animal feed: A review, *J. Mar. Sci. Eng.*, 2020, **8**, 559.

6 X. Xiong, B. Tan, M. Song, P. Ji, K. Kim, Y. Yin and Y. Liu, Nutritional Intervention for the intestinal development and health of weaned pigs, *Front. Vet. Sci.*, 2019, **6**, 46.

7 M. Perez-Rodriguez, R. G. Pellerano, L. Pezza and H. R. Pezza, An overview of the main foodstuff sample preparation technologies for tetracycline residue determination, *Talanta*, 2018, **182**, 1–21.

8 Y. Zhou, Q. Yang, D. Zhang, N. Gan, Q. Li and J. Cuan, Detection and removal of antibiotic tetracycline in water with a highly stable luminescent MOF, *Sens. Actuators, B*, 2018, **262**, 137–143.

9 X. Liu, Q. Ma, X. Feng, R. Li and X. Zhang, A recycled Tb-MOF fluorescent sensing material for highly sensitive and selective detection of tetracycline in milk, *Microchem. J.*, 2021, **170**, 106714.

10 C. Li, X. Zhang, S. Wen, R. Xiang, Y. Han, W. Tang, T. Yue and Z. Li, Interface engineering of zeolite imidazolate framework-8 on two-dimensional Al-metal–organic framework nanoplates enhancing performance for simultaneous capture and sensing tetracyclines, *J. Hazard. Mater.*, 2020, **395**, 122615.

11 L. Wang, W. Xu, W. Y. Li, M. Xie and Y. Q. Zheng, A water-stable uranyl organic framework as a highly selective and sensitive bifunctional luminescent probe for Fe^{3+} and tetracycline hydrochloride, *Chem. – Asian J.*, 2019, **14**, 4246–4254.

12 Z. Gan, X. Hu, X. Xu, W. Zhang, X. Zou, J. Shi, K. Zheng and M. Arslan, A portable test strip based on fluorescent europium-based metal–organic framework for rapid and visual detection of tetracycline in food samples, *Food Chem.*, 2021, **354**, 129501.

13 K. Wu, J. Zheng, Y.-L. Huang, D. Luo, Y. Y. Li, W. Lu and D. Li, $Cr_2O_7^{2-}$ inside Zr/Hf-based metal–organic frameworks: Highly sensitive and selective detection and crystallographic evidence, *J. Mater. Chem. C*, 2020, **8**, 16974–16983.

14 Z. H. Long, D. Luo, K. Wu, Z. Y. Chen, M. M. Wu, X. P. Zhou and D. Li, Superoxide ion and singlet oxygen photogenerated by metalloporphyrin-based metal–organic frameworks for highly efficient and selective photooxidation of a sulfur mustard simulant, *ACS Appl. Mater. Interfaces*, 2021, **13**, 37102–37110.

15 J. Pang, Z. Di, J. S. Qin, S. Yuan, C. T. Lollar, J. Li, P. Zhang, M. Wu, D. Yuan, M. Hong and H. C. Zhou, Precisely embedding active sites into a mesoporous Zr-framework through linker installation for high-efficiency photocatalysis, *J. Am. Chem. Soc.*, 2020, **142**, 15020–15026.

16 Y. C. Qiu, S. Yuan, X. X. Li, D. Y. Du, C. Wang, J. S. Qin, H. F. Drake, Y. Q. Lan, L. Jiang and H. C. Zhou, Face-

sharing Archimedean solids stacking for the construction of mixed-ligand metal–organic frameworks, *J. Am. Chem. Soc.*, 2019, **141**, 13841–13848.

17 B. Li, X. Dong, H. Wang, D. Ma, K. Tan, S. Jensen, B. J. Deibert, J. Butler, J. Cure, Z. Shi, T. Thonhauser, Y. J. Chabal, Y. Han and J. Li, Capture of organic iodides from nuclear waste by metal–organic framework-based molecular traps, *Nat. Commun.*, 2017, **8**, 485.

18 H. Q. Yin and X. B. Yin, Metal–organic frameworks with multiple luminescence emissions: Designs and applications, *Acc. Chem. Res.*, 2020, **53**, 485–495.

19 Y. Cui, Y. Yue, G. Qian and B. Chen, Luminescent functional metal–organic frameworks, *Chem. Rev.*, 2012, **112**, 1126–1162.

20 J. D. ROCCA, D. M. LIU and W. B. LIN, Nanoscale metal–organic frameworks for biomedical imaging and drug delivery, *Acc. Chem. Res.*, 2011, **44**, 957–968.

21 H. Wang, J. Xu, D. S. Zhang, Q. Chen, R. M. Wen, Z. Chang and X. H. Bu, Crystalline capsules: Metal–organic frameworks locked by size-matching ligand bolts, *Angew. Chem., Int. Ed.*, 2015, **54**, 5966–5970.

22 J. K. Jin, K. Wu, X. Y. Liu, G. Q. Huang, Y. L. Huang, D. Luo, M. Xie, Y. Zhao, W. Lu, X. P. Zhou, J. He and D. Li, Building a pyrazole–benzothiadiazole–pyrazole photosensitizer into metal–organic frameworks for photocatalytic aerobic oxidation, *J. Am. Chem. Soc.*, 2021, **143**, 21340–21349.

23 K. Wu, Y.-L. Huang, J. Zheng, D. Luo, M. Xie, Y. Y. Li, W. Lu and D. Li, A microporous shp-topology metal–organic framework with an unprecedented high-nuclearity Co_{10}-cluster for iodine capture and histidine detection, *Mater. Chem. Front.*, 2021, **5**, 4300–4309.

24 R.-J. Wei, H.-G. Zhou, Z.-Y. Zhang, G.-H. Ning and D. Li, Copper(I)–organic frameworks for catalysis: Networking metal clusters with dynamic covalent chemistry, *CCS Chem.*, 2021, **3**, 2045–2053.

25 H. Zeng, M. Xie, T. Wang, R. J. Wei, X. J. Xie, Y. Zhao, W. Lu and D. Li, Orthogonal-array dynamic molecular sieving of propylene/propane mixtures, *Nature*, 2021, **595**, 542–548.

26 B. Wang, Q. Yang, C. Guo, Y. Sun, L. H. Xie and J. R. Li, Stable Zr(IV)-based metal–organic frameworks with predesigned functionalized ligands for highly selective detection of Fe(III) ions in water, *ACS Appl. Mater. Interfaces*, 2017, **9**, 10286–10295.

27 W.-B. Zhong, R.-X. Li, J. Lv, T. He, M.-M. Xu, B. Wang, L.-H. Xie and J.-R. Li, Two isomeric In(III)-MOFs: Unexpected stability difference and selective fluorescence detection of fluoroquinolone antibiotics in water, *Inorg. Chem. Front.*, 2020, **7**, 1161–1171.

28 Y. Zhao, Q. Wang, H. Wang, H. Zhangsun, X. Sun, T. Bu, Y. Liu, W. Wang, Z. Xu and L. Wang, Europium-based metal–organic framework containing characteristic metal chains: A novel turn-on fluorescence sensor for simultaneous high-performance detection and removal of tetracycline, *Sens. Actuators, B*, 2021, **334**, 129610.

29 X. Li, H. Ma, M. Deng, A. Iqbal, X. Liu, B. Li, W. Liu, J. Li and W. Qin, Europium functionalized ratiometric fluorescent transducer silicon nanoparticles based on Fret for the highly sensitive detection of tetracycline, *J. Mater. Chem. C*, 2017, **5**, 2149–2152.

30 H. Q. Yin, X. Y. Wang and X. B. Yin, Rotation restricted emission and antenna effect in single metal–organic frameworks, *J. Am. Chem. Soc.*, 2019, **141**, 15166–15173.

31 Y. Zhao, H. Zeng, X. W. Zhu, W. Lu and D. Li, Metal–organic frameworks as photoluminescent biosensing platforms: Mechanisms and applications, *Chem. Soc. Rev.*, 2021, **50**, 4484–4513.

32 Y. Zhao, M.-Y. Wan, J.-P. Bai, H. Zeng, W. Lu and D. Li, pH-Modulated luminescence switching in a Eu-MOF: Rapid detection of acidic amino acids, *J. Mater. Chem. A*, 2019, **7**, 11127–11133.

33 Y. L. Gai, K. C. Xiong, L. Chen, Y. Bu, X. J. Li, F. L. Jiang and M. C. Hong, Visible and Nir photoluminescence properties of a series of novel lanthanide–organic coordination polymers based on hydroxyquinoline-carboxylate ligands, *Inorg. Chem.*, 2012, **51**, 13128–13137.

34 Y. Ou, W. Zhou, Z. Zhu, F. Ma, R. Zhou, F. Su, L. Zheng, L. Ma and H. Liang, Host differential sensitization toward color/lifetime-tuned lanthanide coordination polymers for optical multiplexing, *Angew. Chem., Int. Ed.*, 2020, **59**, 23810–23816.

35 X. Y. Zhao, J. Wang, Q. S. Yang, D. L. Fu and D. K. Jiang, A hydrostable samarium(III)–MOF sensor for the sensitive and selective detection of tryptophan based on a "dual antenna effect", *Anal. Methods*, 2021, **13**, 3994–4000.

36 J. Ren, Z. Niu, Y. Ye, C. Y. Tsai, S. Liu, Q. Liu, X. Huang, A. Nafady and S. Ma, Second-sphere interaction promoted turn-on fluorescence for selective sensing of organic amines in a Tb^{III}-based macrocyclic framework, *Angew. Chem., Int. Ed.*, 2021, **60**, 23705–23712.

37 R. Plessius, R. Kromhout, A. L. Ramos, M. Ferbinteanu, M. C. Mittelmeijer-Hazeleger, R. Krishna, G. Rothenberg and S. Tanase, Highly selective water adsorption in a lanthanum metal–organic framework, *Chem. – Eur. J.*, 2014, **20**, 7922–7925.

38 Q. Q. Liu, S. H. Zhang, J. Yang and K. F. Yue, A water-stable La–MOF with high fluorescence sensing and supercapacitive performances, *Analyst*, 2019, **144**, 4534–4544.

39 R. R. R. Prasad, S. E. Seidner, D. B. Cordes, M. M. Lozinska, D. M. Dawson, M. J. Thompson, T. Düren, K. K. Chakarova, M. Y. Mihaylov, K. I. Hadjiivanov, F. Hoffmann, A. M. Z. Slawin, S. E. Ashbrook, M. L. Clarke and P. A. Wright, STA-27, a porous Lewis acidic scandium MOF with an unexpected topology type prepared with 2,3,5,6-tetrakis(4-carboxyphenyl)pyrazine, *J. Mater. Chem. A*, 2019, **7**, 5685–5701.

40 M. Lammert, H. Reinsch, C. A. Murray, M. T. Wharmby, H. Terraschke and N. Stock, Synthesis and structure of Zr(IV)- and Ce(IV)-based CAU-24 with 1,2,4,5-tetrakis(4-carboxyphenyl)benzene, *Dalton Trans.*, 2016, **45**, 18822–18826.

41 X. P. Wu, L. Gagliardi and D. G. Truhlar, Cerium metal–organic framework for photocatalysis, *J. Am. Chem. Soc.*, 2018, **140**, 7904–7912.
42 L.-J. Han, Y.-J. Kong, X.-M. Zhang, G.-Z. Hou, H.-C. Chen and H.-G. Zheng, Fluorescence recognition of adenosine triphosphate and uric acid by two Eu-based metal–organic frameworks, *J. Mater. Chem. C*, 2021, **9**, 6051–6061.
43 W. Liu, X. Huang, C. Xu, C. Chen, L. Yang, W. Dou, W. Chen, H. Yang and W. Liu, A multi-responsive regenerable europium–organic framework luminescent sensor for Fe^{3+}, Cr^{VI} anions, and picric acid, *Chem. – Eur. J.*, 2016, **22**, 18769–18776.
44 Y. Jiang, L. Sun, J. Du, Y. Liu, H. Shi, Z. Liang and J. Li, Multifunctional zinc metal–organic framework based on designed H_4TCPP ligand with aggregation-induced emission effect: CO_2 adsorption, luminescence, and sensing property, *Cryst. Growth Des.*, 2017, **17**, 2090–2096.
45 N. B. Shustova, B. D. McCarthy and M. Dinca, Turn-on fluorescence in tetraphenylethylene-based metal–organic frameworks: An alternative to aggregation-induced emission, *J. Am. Chem. Soc.*, 2011, **133**, 20126–20129.
46 N. Wang, J. Zhang, X. D. Xu and S. Feng, Turn-on fluorescence in a pyridine-decorated tetraphenylethylene: The cooperative effect of coordination-driven rigidification and silver ion induced aggregation, *Dalton Trans.*, 2020, **49**, 1883–1890.
47 Y. Zhao, H. Zeng, K. Wu, D. Luo, X.-W. Zhu, W. Lu and D. Li, A pH-regulated ratiometric luminescence Eu-MOF for rapid detection of toxic mycotoxin in moldy sugarcane, *J. Mater. Chem. C*, 2020, **8**, 4385–4391.
48 J. M. Zhou, W. Shi, N. Xu and P. Cheng, Highly selective luminescent sensing of fluoride and organic small-molecule pollutants based on novel lanthanide metal–organic frameworks, *Inorg. Chem.*, 2013, **52**, 8082–8090.
49 F. Weigend, Accurate Coulomb-fitting basis sets for H to Rn, *Phys. Chem. Chem. Phys.*, 2006, **8**, 1057–1065.
50 F. Zu, F. Yan, Z. Bai, J. Xu, Y. Wang, Y. Huang and X. Zhou, The quenching of the fluorescence of carbon dots: A review on mechanisms and applications, *Microchim. Acta*, 2017, **184**, 1899–1914.
51 Y. B. Wei, M. J. Wang, D. Luo, Y. L. Huang, M. Xie, W. G. Lu, X. G. Shu and D. Li, Ultrasensitive and highly selective detection of formaldehyde via an adenine-based biological metal–organic framework, *Mater. Chem. Front.*, 2021, **5**, 2416–2424.